Modeling cavitation erosion using non-homogeneous gamma process

Q. Chatenet, E. Remy, M. Gagnon, Mitra Fouladirad, A.S. Tahan

Version of Record: https://www.sciencedirect.com/science/article/pii/S0951832021002106
Manuscript_a830a7e10ee1a20d88435b7b3c5f3946

Modeling cavitation erosion using non-homogeneous gamma process

Q Chatenet[a,*], E Remy[b], M Gagnon[c], M Fouladirad[d], A S Tahan[a]

[a] *École de Technologie Supérieure, 1100 Rue Notre-Dame Ouest, H3C 1K3, Montréal, QC, Canada*
[b] *EDF R&D, 6 Quai Watier, 78401 Chatou Cedex, France*
[c] *Institut de Recherche d'Hydro Québec, 1800 Boulevard Lionel-Boulet, J3X 1S1, Varennes, QC, Canada*
[d] *Université de Technologie de Troyes, 12 Rue Marie Curie, 10300 Troyes, France*

Abstract

Although hydroelectric generating units are highly reliable, being able to accurately model their degradation level represents a real asset in industrial and financial risk management. This paper presents and models a common degradation phenomenon observed on hydraulic Francis turbine runners: erosive cavitation. It gives an application of stochastic processes for degradation modeling framework in presence of real laboratory experimental data. For degradation modeling, a non homogeneous gamma process is proposed. The model calibration is explained and asymptotic confidence intervals for the model estimate are assessed. Because of the limited size of available dataset, bootstrap techniques are also used to evaluate statistical estimation uncertainties on the model parameters. These uncertainties on the degradation model are then propagated in order to analyze how they impact the distribution of the system lifetime, characterized by the hitting time for a given degradation threshold.

Keywords: degradation modeling, gamma process, bootstrap, estimation uncertainty, delta method, erosive cavitation, lifetime estimation

1. Introduction

1.1. Industrial context

Component reliability represents a significant aspect of industrial asset management for energy producers who operate generating units in highly competitive market. In this context, being able to build robust reliability models is crucial to the ultimate success of maintenance program [1]. For this purpose, engineers and analysts may rely on existing probabilistic models developed in literature [2, 3]. For complex systems such as hydroelectric power stations (which includes: turbine runner, generator, civil, ...), available data can be limited due to the systems' high reliability but also because of the effort needed to collect degradation data. The resulting reliability model may thus suffer from a lack of accuracy and the assessment of statistical

*Corresponding author
Email address: quentin.chatenet.1@etsmtl.net (Q Chatenet)

estimation uncertainties may become a real challenge in order to evaluate model performance and robustness. Moreover, having a good knowledge of these uncertainties gives the analyst a better representation of possible future system behavior and allows him, for example, to make risk-informed decisions regarding operation or maintenance policies.

Nomenclature

$\mathbb{R}_+^*$	set of positive real numbers
$\mathbf{D}_{obs}$	set of observed degradation data
$x_{i,j}$	degradation level of component j at instant $t_{i,j}$
$\delta_{i,j}$	increment of degradation between two successive instants
u	gamma process rate parameter
v	gamma process shape parameter
$\boldsymbol{\theta}$	set of gamma process parameters
n_j	path size
m	number of paths
N	total number of observations
$\mathcal{L}$	likelihood function
ℓ	log-likelihood function
Φ	CDF of the standard Gaussian distribution
P_Y^q	quantile of order q of distribution of Y
T_ρ	first hitting time of degradation at level ρ
HGP	homogeneous gamma process
NHGP	non-homogeneous gamma process
BS	Birnbaum-Saunders
ML	maximum likelihood
MLE	maximum likelihood estimation
EB	Efron bootstrap
PB	parametric bootstrap
MBB	moving block bootstrap
DM	delta method
GSS	gamma sequential sampling
MSE	mean squared error

1.2. Degradation phenomenon

Cavitation erosion is the physical degradation process studied in this paper [4]. This phenomenon occurs when the local static pressure of water is below its vapor pressure at a given temperature. For high velocity regions on the runner blade, the local low pressure can result in the formation of small vapor bubbles which then collapse suddenly. If the created bubbles implode on solid surfaces, such as the runner blades, surfaces eventually end up with pitting erosion [5]. Cavitation results in noise, vibration, and alteration of the surface geometry of the blade. In the end it may lead to loss in the turbine efficiency [6]. Over time, a Francis runner exposed to erosive cavitation will loose material which requires costly periodic inspections and repairs. A relevant technique to quantify this degradation in laboratory consists of measuring the mass of the specimen and thus deduce the material loss during the experiment. In order to optimize maintenance operations and to reduce periods of outage, there is a need for accurate degradation prediction. While progress has been made during the last decade, computational fluid dynamics simulations still face challenges to anticipate cavitation erosion. Indeed, recent studies on the prediction of cavitation erosion have shown satisfying qualitative results, but stress that future work is needed to produce convincing quantitative assessments [7]. In particular, numerical models can predict the blade regions affected by erosive cavitation but are still not able to produce robust results about the cavitation intensity and consequently the resulting material loss [8]. Although the following methodology focuses on cavitation erosion, a similar approach may be applied to other cumulative and monotonic degradation mechanism.

1.3. Objectives

To perform accurate degradation prediction, an analyst must rely on a realistic model which ideally integrates the physics of degradation, the characteristics of the operating environment and the impact of the usage [9, 10]. Accurate degradation modeling is made possible through the use of degradation data collected by laboratory experiments, monitoring or during inspections of the system. These models allow the prediction of the lifetime of the system, characterized by the first hitting time for a given degradation level threshold. In the case of cavitation erosion, because of the natural variability of the physical phenomenon and the large number of unknown influencing factors, we consider that the mechanism is random. For these reasons, we discarded deterministic models in favor of probabilistic ones.

This paper aims to propose a stochastic model describing the erosive cavitation phenomenon encountered on industrial equipment. The modeling is based on real data obtained under controlled environment in laboratory. The main issue is that the dataset is very small and the major statistical methods applied for model calibration and validation are based on large size data. This problem is bypassed by the bootstrap methods which enrich the dataset by generating a large set of resampled data. The bootstrap behavior for this specific industrial framework is studied and the advantages and limits of the bootstrap for this particular industrial case is discussed. Confidence intervals for parameters estimation are proposed. A risk-informed

metric, evaluating the influence of these confidence intervals on the system lifetime distribution (estimating the first hitting time for a given degradation level) is proposed. This latter allows to compare the different statistical techniques based on asymptotic and non-asymptotic results. Although the methods we used in this paper are standard, this study is conducted on real industrial data and propose to construct not only confidence intervals on model parameters but to propagate them to a reliability performance criterion of interest (while most papers limit themselves to the estimation of model uncertainties).

The paper is structured as follows. First, we provide a brief introduction of probabilistic degradation models and present the particular case of the model we chose to conduct this study. Next, we present the methodology used to construct confidence intervals on model parameters: (i) theoretical asymptotic properties of maximum likelihood estimators and (ii) bootstrap methods. Then, we apply the previous techniques on a real dataset and discuss the results. Finally, some of the challenges faced for degradation modeling are discussed, along with suggestions for further work.

2. Degradation models

In health indicator prognostic, when only failure times are known, black box models such as lifetime models are used to analyze the behavior of the system. To take advantage of the available information provided by deterioration data (collected during system's monitoring or inspection), stochastic processes are suitable candidates to describe the evolution over time of the health indicator. Indeed, degradation data can be seen as a collection of random variables (increments of degradation), and can be modeled in terms of a stochastic process. Another applicable tool would be the use of regression models also known as "degradation path models" [10, 11].

2.1. Degradation path models

Let us denote $x_{i,j}$, $i = 1 \dots n$, with $0 = x_{0,j} \leq x_{1,j} \leq \cdots \leq x_{n,j}$, the observed degradation level related to component j, $j = 1 \dots m$, at instant $t_{i,j}$, where $0 = t_{0,j} < t_{1,j} < \cdots < t_{n,j}$. For regression models, the successive degradation levels are considered as independent observations which means the dynamics of degradation and its cumulative property over the time are overlooked, as well as the way degradation values are collected and organized. Likewise, random effect models can be suitable for degradation exhibiting unexplained heterogeneity within a similar component population. These models are often used in presence of uncontrolled environment (which is not the case for the dataset studied in this paper, which was obtained during laboratory experiments). In contrast, stochastic processes model the degradation path variability by considering the dynamics and the cumulative property of degradation using its increments between two successive instants. For these reasons, regression models are discarded in the remaining of this paper.

2.2. Stochastic processes

As pointed out in the survey by Noortwijk, Markov stochastic processes are well suited for modeling the temporal variability of degradation [12, 13]. In the context of cumulative degradation, it is relevant to consider processes belonging to the Markov process family as the future states depend only upon the current state and not on previous states [14] which is the case for two successive measurements of erosive cavitation.

In the Markov process class, a distinction is made between processes having a finite or countable state space and infinite state space: cavitation erosion measurements lie in the infinite state case as the degradation level is measured using the mass loss of the specimen which can take theoretically an infinite number of values (uncountable). Likewise, we can find discrete-time or continuous-time processes as depicted by Karlin [15]. In the framework of our study, we consider the physical phenomenon as a time-continuous process even if degradation observations are carried out at discrete times. Many useful continuous-time processes can be considered to model degradation such as the Brownian motion with drift (or Wiener process) [16, 17], the compound Poisson process [18], the inverse Gaussian process [19] and the gamma process [20]. A characteristic feature of the Wiener process – in the context of degradation – is that the deterioration may alternately increase and decrease over time (non-monotonic), even with an increasing trend, called Brownian motion with drift (see review by Guan et al. [21] and application with measurement errors in Whitmore [22]). As the degradation studied in this paper is cumulative and strictly monotonic, inverse Gaussian process and gamma process are good candidates because of their independent non-negative increments [23, 24]. With both these two processes, paths can be thought as the accumulation over time of an infinite number of tiny increments. These features make these processes relevant to model gradual damage accumulating over time. IG process was used by Ye and Chen [25] because of its inherent flexibility and the possibility to incorporate covariates and random effects. Meanwhile, Ye and Chen [25] stress IG process is not well received by reliability engineers or analysts compared to Wiener or gamma processes due to its unclear degradation physical meaning. More over, inverse Gaussian process is often considered when Wiener or gamma process fail to model degradation data. Other Markov processes can be found in a reliability context such as diffusion processes. In order to better control mean and variance of a given degradation process, Deng et al. [26] used an Ornstein-Uhlenbeck process which lies in the diffusion process family. This process shares some similarities with the Wiener process with drift, such as the ability to model degradation having temporary fluctuations while the overall trend is increasing. Because the studied degradation is monotonic and cumulative, these processes were discarded to prefer a monotonic process for the remaining of the paper. Since the aim is to derive a calibration, estimation and prediction methodology in presence of small size data and highlight the interest of time dependent average and volatility, gamma process as a monotonic process is used to show the implementation of the whole methodology. Any other Lévy subordinator or non stationary non decreasing stochastic process could be chosen.

2.3. Model description

In its homogeneous form, the gamma process has a linear average trend but the non-homogeneous gamma process can have convex or concave average trends. This is more flexible to fit a given average trend but it does not satisfy the stationarity property. Castanier et al. [27] used it in the framework of condition-based maintenance. In de Jonge [28], Deloux et al. [29] and Zhu et al. [30], the gamma process is enriched with additional random shocks or/and covariates to describe a more complex behavior undergoing environmental changes. In presence of measurements, the fitting and calibration is one of the major issues and the parameters estimation is the main challenge. The latter is addressed in Wang [31] and Kahle et al. [3] under different hypotheses on data or model. Ling et al. [24] used and estimated parameters of a non-homogeneous gamma process to study the evolution of the remaining useful life of light emitting diodes under stress conditions. In addition, they evaluated uncertainties of model parameter estimations in the case of shape function following an inverse power law. When degradation data contain noise or measurement errors, leading to non-strictly monotonic trend, Le Son et al. [32] used a Gibbs sampling technique to filter signal and then used a non-homogeneous gamma process to model hidden degradation data for the same purpose; Lu et al. [33] preferred the use of the Genz transform and quasi-Monte Carlo method.

Abdel-Hameed [20] was the first to use gamma process (GP) to model degradation occurring randomly in time. Van Noortwijk [12] and Alaswad and Xiang [13], in their respective survey, noted the ability of gamma process to model gradual damage monotonically accumulating over time. In particular, Cholette et al. [34] and Nystad et al. [35] used GP to model systems subject to erosion. The definition given by Van Noortwijk [12] describes gamma process as a stochastic process with independent, non-negative increments having a gamma distribution with an identical scale parameter.

A positive random quantity X has a gamma distribution, denoted $Ga(u, v)$, where $u, v > 0$ are the rate parameter and the shape parameter, respectively, if its probability density function (PDF) is given by:

$$f_X(x|u, v) = Ga(x|u, v) = \frac{u^v}{\Gamma(v)} x^{v-1} \exp(-ux) I_{\mathbb{R}_+^*}(x), \tag{1}$$

where $I_A(x) = 1$ for $x \in A$ and $I_A(x) = 0$ for $x \notin A$, $\Gamma(a)$ is the incomplete gamma function for $a > 0$ [36] and $\mathbb{R}_+^*$ the set of positive real numbers. Note that another standard parameterization of the gamma distribution in the literature is (α, β) with $\beta = 1/u$ and $\alpha = v$. In that case, β is called scale parameter and α the shape parameter.

The gamma process $\{X(t), t \geq 0\}$ with rate parameter $u > 0$ and shape function $v(t) > 0$ has the following properties:

- $X(0) = 0$,
- $X(\tau) - X(t) \sim Ga(u, v(\tau) - v(t))$ for all $\tau > t > 0$,

- $X(t)$ has independent non-overlapping increments.

Note that v must be a non-decreasing, right-continuous, real-valued function on $\mathbb{R}_+$ with $v(0) = 0$. The expectation and the variance of gamma process with parameters u and $v(t)$ are the following:

$$\mathbb{E}(X(t)) = \frac{v(t)}{u}, \qquad \mathbb{V}(X(t)) = \frac{v(t)}{u^2}. \tag{2}$$

The shape function $v(t)$ expresses how the mean degradation increases over time. A standard choice is $v(t) = ct^b$ with $c, b > 0$ [3]. Empirical studies and engineering knowledge show the expected degradation over time is often proportional to a power function [12]. When $b = 1$, the gamma process is said to be homogeneous (HGP, or stationary); for $b \neq 1$, the gamma process is non-homogeneous (NHGP, or non-stationary). In their study, Park and Padgett [37] identified an appropriate value of b based on the Akaike Information Criterion, which is a standard statistical indicator for model selection. In the remaining of the paper, we chose to use a power function for v. Another standard shape function could have been the exponential one: $v(t) = e^{-ct} - 1$, with $c > 0$, but because of the degradation behavior studied in this paper (see section 4), we decided to discard this shape function.

2.4. Maximum likelihood estimation of model parameters

In order to model degradation phenomenon using gamma process, appropriate statistical methods are required for the model parameters' estimation. Two of the most common techniques are the Maximum Likelihood method (ML) and the Method of Moments (MM). MM is preferred when power $b \neq 1$ in $v(t)$ is known and for i.d. time increments: in that case, the NHGP can be transformed into a HGP which leads to simpler parameters' estimation using MM [12]. MM being explicit, it can be used as a starting point for ML method which may require an iterative optimization procedure. Meanwhile, when b needs to be determined, ML is more convenient than MM. In our case study, preliminary statistical regression showed a good fit for power function (see degradation path in Figure 3). As we had no information on parameter b, we decided to use the ML method. Let us introduce this estimation method.

Let us suppose we observe m independent paths following the same stochastic process. Here, m expresses the number of laboratory experiments performed (it could also express m different and independent systems on which we observe one degradation path). Let n_j denote the number of successive observations taken during experiment j, $1 \leq j \leq m$. Then, the j^{th} degradation path is observed $n_j + 1$ times at instants $t_{0,j} < t_{1,j} < \ldots < t_{n_j,j}$. We adopt the following notations in the remaining of the paper, for all $1 \leq j \leq m$ (see Fig. 1):

- $t_{0,j} = t_0 = 0$;
- $x_{0,j} = 0$, which means at t_0 there is no degradation;

- $\delta_{i,j} = x_{i+1,j} - x_{i,j}$: the increment of degradation between two successive measurement instants $t_{i,j}$ and $t_{i+1,j}$;
- $\mathbf{D}_{obs} = \cup_{j=1}^{m} \cup_{i=0}^{n_j} \{(t_{i,j}, x_{i,j})\} = \cup_{j=1}^{m} \cup_{i=0}^{n_j-1} \{(t_{i,j}, t_{i+1,j}, \delta_{i,j})\}$: the set of all observed degradation data, organized in m independent paths with n_j observations, $1 \leq j \leq m$.

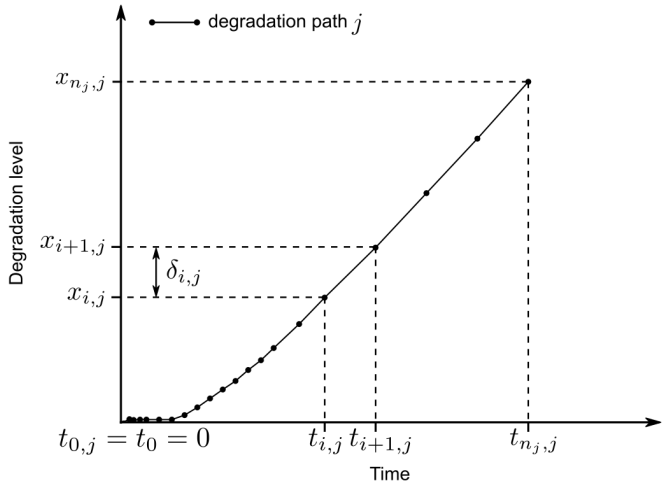

Figure 1: Data notation example.

In our case, since the degradation measurements come from experiments performed in laboratory (see section 4), under controlled conditions, we consider the measurement error is negligible compared to the natural variability of the degradation phenomenon (see [22] for stochastic process considering measurement error). Note that for a given experiment j, $1 \leq j \leq m$, increments $\delta_{i,j}$, $0 \leq i \leq n_j - 1$, are independent but non-identically distributed (i.non-i.d) since they depend on the (possibly non-uniform) width of time intervals $[t_{i,j}, t_{i+1,j}]$ between successive measurements. Because of this property, the classical graphical tools and goodness of fit tests are not applicable. Indeed, in the non-homogeneous case, each degradation increment follows a different gamma distribution described, in particular, by instants $t_{i,j}$ and $t_{i+1,j}$ (not δt_i anymore). Other classes of classification tools could be studied but due to their originality, for their application their whole background should be recalled and defined which goes further than the main objective of this paper.

The ML method consists of identifying the model parameter $\hat{\boldsymbol{\theta}} = (\hat{u}, \hat{c}, \hat{b})$ values which maximize the likelihood function $\mathcal{L}$ given observed data $\mathbf{D}_{obs}$. Intuitively, it selects the parameters' values that make the data most probable. The gamma process likelihood function $\mathcal{L}$ is given in equation (3) (see [12]). For convenience, we chose to maximize the log-likelihood function ℓ in equation (4).; because of strictly increasing behavior of the log function, log-likelihood achieves its maximum value at the same points as the function itself.

$$\begin{aligned}\mathcal{L}(\boldsymbol{\theta}|\mathbf{D}_{obs}) = \mathcal{L}(u,c,b|\mathbf{D}_{obs}) &= \prod_{j=1}^{m}\prod_{i=1}^{n_j} Ga\left(\delta_{i,j}|u, v(t_{i,j}) - v(t_{i-1,j})\right) \\ &= \prod_{j=1}^{m}\prod_{i=1}^{n_j} \frac{u^{c[t^b_{i,j}-t^b_{i-1,j}]}}{\Gamma(c[t^b_{i,j}-t^b_{i-1,j}])}\delta_{i,j}^{c[t^b_{i,j}-t^b_{i-1,j}]-1}e^{-u\delta_{i,j}}.\end{aligned} \tag{3}$$

$$\begin{aligned}\ell(\boldsymbol{\theta}|\mathbf{D}_{obs}) &= \log\left(\mathcal{L}(u,c,b|\mathbf{D}_{obs})\right) \\ &= \sum_{j=1}^{m}\sum_{i=1}^{n_j} c[t^b_{i,j}-t^b_{i-1,j}]\log(u) - \log\left[\Gamma\left(c[t^b_{i,j}-t^b_{i-1,j}]\right)\right] \\ &+ \left(c[t^b_{i,j}-t^b_{i-1,j}]-1\right)\log(\delta_{i,j}) - u\delta_{i,j}.\end{aligned} \tag{4}$$

By differentiating ℓ with respect to the three parameters, the Maximum Likelihood Estimator (MLE) $\hat{\boldsymbol{\theta}}_{ML} = (\hat{u}_{ML}, \hat{c}_{ML}, \hat{b}_{ML})$ of true unknown parameters $\boldsymbol{\theta} = (u, c, b)$ consists in the solution of the following set of three non-linear equations:

$$\hat{u}_{ML} = \hat{c}_{ML}\frac{\sum_{j=1}^{m}\sum_{i=1}^{n_j} t_{i,j}^{\hat{b}_{ML}} - t_{i-1,j}^{\hat{b}_{ML}}}{\sum_{j=1}^{m}\sum_{i=1}^{n_j}\delta_{i,j}} = \hat{c}_{ML}\frac{\sum_{j=1}^{m} t_{n_j,j}^{\hat{b}_{ML}}}{\sum_{j=1}^{m} x_{n_j,j}}, \tag{5}$$

$$\sum_{j=1}^{m}\sum_{i=1}^{n_j}\left[t_{i,j}^{\hat{b}_{ML}} - t_{i-1,j}^{\hat{b}_{ML}}\right]\left\{\psi\left(\hat{c}_{ML}\left[t_{i,j}^{\hat{b}_{ML}} - t_{i-1,j}^{\hat{b}_{ML}}\right]\right) - \log(\delta_{i,j})\right\} = \sum_{j=1}^{m}(t_{n_j,j}^{\hat{b}_{ML}})\log(\hat{u}_{ML}), \tag{6}$$

$$\begin{aligned}&\sum_{j=1}^{m}\sum_{i=1}^{n_j}\hat{c}_{ML}\left[t_{i,j}^{\hat{b}_{ML}}\log(t_{i,j}) - t_{i-1,j}^{\hat{b}_{ML}}\log(t_{i-1,j})\right]\left[\psi\left(\hat{c}_{ML}\left[t_{i,j}^{\hat{b}_{ML}} - t_{i-1,j}^{\hat{b}_{ML}}\right]\right) - \log(\delta_{i,j})\right] \\ &= \sum_{j=1}^{m}\left(\hat{c}_{ML}t_{n_j,j}^{\hat{b}_{ML}}\log(t_{n_j,j})\right)\log\left(\hat{u}_{ML}\right),\end{aligned} \tag{7}$$

where function $\psi(a)$, the digamma function, is the derivative of the logarithm of the gamma function:

$$\psi(a) = \frac{\Gamma'(a)}{\Gamma(a)} = \frac{d}{da}\log\Gamma(a). \tag{8}$$

Hence, $\hat{c}_{ML}$ and $\hat{b}_{ML}$ can be either numerically computed by solving equations (6) and (7) (replacing $\hat{u}_{ML}$ by its expression given in (5) which is function of $\hat{c}_{ML}$ and $\hat{b}_{ML}$) or by first computing the MLE for c and b and then computing $\hat{u}_{ML}$ using equation (5). Both methods are numerical and imply an optimization using proper computing tools to solve equations (5), (6) and (7). We chose to use the root finding method `hybr` which relies on MINPACK's hybrd and hybrj routines (modified Powell method, see `scipy.optimize.root` for more details).

2.5. Distribution functions of the component time to failure

A system is often considered to be failed as soon as its degradation level is beyond a given threshold ρ. Let T_ρ be the time at which failure occurs which is the first hitting time of degradation level ρ: $T_\rho = \inf\{t \geq 0, X(t) \geq \rho\}$. Since the degradation increments follow gamma distributions (see equation (1)), as it is mentioned in [12], the cumulative distribution function (CDF) of T_ρ can be written as follows:

$$\begin{aligned} \mathbb{F}_{T_\rho}(t|u, v(t)) = \mathbb{P}(T_\rho \leq t) &= \mathbb{P}(X(t) \geq \rho) \\ &= \int_{x=\rho}^{\infty} f_{X(t)}(x|u, v(t))\, dx = \frac{\Gamma(v(t), \rho)}{\Gamma(v(t))}, \end{aligned} \tag{9}$$

where $\Gamma(\cdot, \cdot)$ is the upper incomplete gamma function. Moreover since the shape function v considered in our study is differentiable, the PDF of T_ρ becomes:

$$\forall t \geq 0, \quad f_{T_\rho}(t|u, v(t)) = \frac{v'(t)}{\Gamma(v(t))} \int_{u\rho}^{\infty} \{\log(z) - \psi(v(t))\} z^{v(t)-1} e^{-z}\, dz. \tag{10}$$

Note that other expressions for the CDF of hitting time T_ρ can be found in [38]. Meanwhile, because of the gamma function behavior, computing equation (10) can be tricky in practice [37] even if the expression gives the exact distribution of the first passage time to threshold ρ. To solve this issue, Park and Padgett [37] introduced the Birnbaum-Saunders distribution [39] to approximate the above distribution in the case of HGP. This approximation of the hitting time CDF, denoted $\mathbb{F}_{BS}$, is simpler than the exact expression of $\mathbb{F}_{T_\rho}$. Paroissin and Salami [38] proved the approximation is also valid for non linear gamma shape function v. Equation (9) can be then approximated by the following formula:

$$\begin{aligned} \mathbb{F}_{T_\rho}(t|u, v(t)) = \mathbb{P}(T_\rho \leq t) &\simeq \mathbb{F}_{BS}(t|u, v(t)), \\ \text{with } \mathbb{F}_{BS}(t|u, v(t)) &= -\Phi\left(\frac{u\rho - v(t)}{\sqrt{v(t)}}\right) \\ &= \Phi\left[\sqrt{u\rho}\left(\sqrt{\frac{v(t)}{u\rho}} - \sqrt{\frac{u\rho}{v(t)}}\right)\right], \end{aligned} \tag{11}$$

where Φ is the CDF of the standard Gaussian distribution.

3. Model parameters' estimations uncertainties

Determining confidence intervals for model parameters is crucial to evaluate the confidence put in the lifetime prediction by the analyst. Even if stochastic processes, such as gamma process, can provide a good mathematical framework for degradation modeling, MLE (among other statistical estimations) is only based on limited information. In our case, information comes from the cumulative degradation measurements,

observed over a specific period of time with a few data points. Thus, different degradation paths may result in different estimations of model parameters. To reflect statistical uncertainty and phenomenon variability, confidence interval (CI) including the true (unknown) parameter $\boldsymbol{\theta}$ should be then computed. Figure 2 shows the approach used to obtain uncertainties on both estimations of model parameter and hitting time distribution from methods introduced in the following sections.

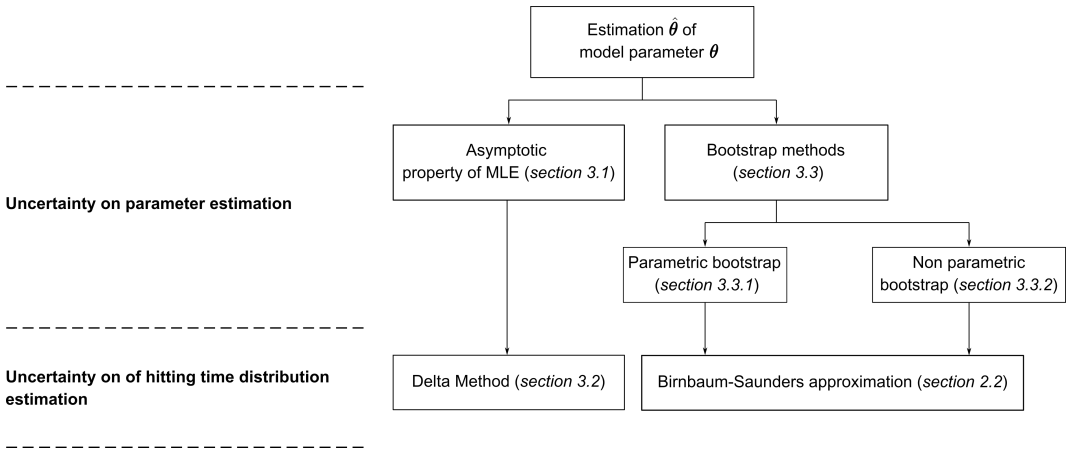

Figure 2: Approach to obtain uncertainties on both estimations of model parameter and associated hitting time distribution.

3.1. Asymptotic confidence intervals approximation using the MLE convergence property

As $N = \sum_{j=1}^{m} n_j$, the total number of observations, gets larger, the log-likelihood function ℓ shows two interesting properties. First, $\ell(\boldsymbol{\theta}|\mathbf{D}_{obs})$ becomes more sharply peaked around $\hat{\boldsymbol{\theta}}_{ML}$. Second, $\ell(\boldsymbol{\theta}|\mathbf{D}_{obs})$ becomes more symmetrical around $\hat{\boldsymbol{\theta}}_{ML}$. This asymptotic behavior shows basically that as the sample size of observations $\mathbf{D}_{obs}$ grows, we are becoming more confident that $\hat{\boldsymbol{\theta}}_{ML}$ lies close to the true parameter $\boldsymbol{\theta}$. Thus, the curvature of the likelihood (*i.e.* the second derivative of $\ell(\boldsymbol{\theta}|\mathbf{D}_{obs})$ with respect to $\boldsymbol{\theta}$) is an important characteristic of $\boldsymbol{\theta}$. This property is the basis for constructing confidence intervals for the unknown parameter $\boldsymbol{\theta}$. These assertions are supported by the asymptotic property of first and second derivative of $\ell(\boldsymbol{\theta}|\mathbf{D}_{obs})$ given by the central limit theorem (CLT) [40]. Hoadley [41] gives conditions under which asymptotic convergence of MLE can be demonstrated in the case of independent but not identically distributed (i.non-i.d.) observations which is the case for our study case (see sections 2.4 and 4). To lighten the notation, $\ell(\boldsymbol{\theta}|\mathbf{D}_{obs})$ will be simply noted $\ell(\boldsymbol{\theta})$. In the context of MLE, the asymptotic normality derived by Rao [42] gives:

$$(\hat{\boldsymbol{\theta}}_{ML} - \boldsymbol{\theta}) \xrightarrow{d} \mathcal{N}\left(0, I^{-1}(\boldsymbol{\theta})\right), \tag{12}$$

with $I(\boldsymbol{\theta})$ the expected Fisher information matrix. Also, $\xrightarrow{d}$ denotes convergence in law when N goes to infinity. Because computing the expected Fisher information is not possible when its analytic expression is

unavailable, we used the observed Fisher information $J(\boldsymbol{\theta})$, introduced by Efron and Hinkley [43], which is given by the following expression:

$$J(\boldsymbol{\theta}) = -\nabla^2 \ell(\boldsymbol{\theta}). \tag{13}$$

The gradient vector of the first partial derivatives of log-likelihood function $\ell(\boldsymbol{\theta})$ of the gamma process can be written:

$$\nabla \ell(\boldsymbol{\theta}) = \begin{pmatrix} \frac{\partial \ell(\boldsymbol{\theta})}{\partial u} \\ \frac{\partial \ell(\boldsymbol{\theta})}{\partial c} \\ \frac{\partial \ell(\boldsymbol{\theta})}{\partial b} \end{pmatrix}, \tag{14}$$

and the Hessian matrix with the second partial derivatives of log-likelihood function $\ell(\boldsymbol{\theta})$ is the following:

$$\nabla^2 \ell(\boldsymbol{\theta}) = \begin{pmatrix} \frac{\partial^2 \ell(\boldsymbol{\theta})}{\partial u^2} & \frac{\partial^2 \ell(\boldsymbol{\theta})}{\partial u \partial c} & \frac{\partial^2 \ell(\boldsymbol{\theta})}{\partial u \partial b} \\ \frac{\partial^2 \ell(\boldsymbol{\theta})}{\partial c \partial u} & \frac{\partial \ell(\boldsymbol{\theta})}{\partial c^2} & \frac{\partial^2 \ell(\boldsymbol{\theta})}{\partial c \partial b} \\ \frac{\partial^2 \ell(\boldsymbol{\theta})}{\partial b \partial u} & \frac{\partial \ell(\boldsymbol{\theta})}{\partial b \partial c} & \frac{\partial^2 \ell(\boldsymbol{\theta})}{\partial b^2} \end{pmatrix}. \tag{15}$$

It is possible to compute confidence intervals on $\boldsymbol{\theta}$ using the asymptotic normality of MLE. The asymptotic approximate symmetric two-sided confidence intervals at level $1-\alpha$, $0 < \alpha < 1$, for $\boldsymbol{\theta}$ considering each of its components $\boldsymbol{\theta}_i$ are:

$$\left[\hat{\boldsymbol{\theta}}_{ML,i} - s\sqrt{\left(J(\hat{\boldsymbol{\theta}})^{-1}\right)_{ii}};\ \hat{\boldsymbol{\theta}}_{ML,i} + s\sqrt{\left(J(\hat{\boldsymbol{\theta}})^{-1}\right)_{ii}} \right], \tag{16}$$

where $s = \Phi\left(1 - \frac{\alpha}{2}\right)$ (*e.g.*: 1.96 for $1-\alpha = 95\%$ confidence level).

3.2. Delta method

The delta method (DM), also called the method of propagation of error, allows analyst to derive the variance of a transformation of one or more random variables [44]. DM states that the asymptotic behavior of functions over a random variable can be approximated if the random variable is itself asymptotically normal. In particular, DM can be used to derive percentiles of hitting time distribution from estimated parameters and their respective CI. To our knowledge, we are the first to apply delta method in the framework of gamma processes.

First, as described in [45], let us consider the sequence $(W_n)_{n\in\mathbb{N}}$ of $\mathbb{R}^p$-valued random vectors. Assume there exist $\mu_W \in \mathbb{R}^p$ and Σ a $p \times p$ definite positive matrix such that:

$$\sqrt{n}(W_n - \mu_W) \xrightarrow[n\to\infty]{d} \mathcal{N}(0, \Sigma). \tag{17}$$

Consider r real functions $g_1, \ldots, g_r$ with continuous first partial derivatives in μ_W, where at least one of these derivatives is non-zero. For $i \in \{1, \ldots, r\}$ and for any $n \in \mathbb{N}^*$, set $Z_{i,n} = g_i(W_n)$, $Z_n = (Z_{1,n}, \ldots, Z_{r,n})^T$ and $\mu_Z = (g_1(\mu_W), \ldots, g_r(\mu_W))^T$. Then the sequence $(Z_n)_{n\in\mathbb{N}^*}$ is also asymptotically normal:

$$\sqrt{n}(Z_n - \mu_Z) \xrightarrow[n\to\infty]{d} \mathcal{N}(0, K\Sigma K^T), \tag{18}$$

where K is the $r \times p$ matrix with elements $k_{i,j} = \dfrac{dg_i}{dw_j}$ for $i \in \{1, \ldots, r\}$ and $j \in \{1, \ldots, p\}$.

In this study, we are interested in how estimation uncertainties on $\boldsymbol{\theta}$ may impact the distribution of T_ρ, in particular its percentiles of order q, $0 < q < 1$, given by: $P^q_{T_\rho} = \mathbb{F}^{-1}_{T_\rho}(q|\boldsymbol{\theta}) \approx \mathbb{F}^{-1}_{BS}(q|\boldsymbol{\theta})$. If we consider the hypothesis of convergence given in equation (12) is satisfied, therefore DM can be applied. Thus when $N = \sum_{j=1}^m n_j$ is large enough, $g(\hat{\boldsymbol{\theta}}_{ML})$ follows the normal distribution: $\mathcal{N}\left(g(\boldsymbol{\theta}), J_g(\boldsymbol{\theta})J^{-1}(\hat{\boldsymbol{\theta}}_{ML})J_g(\boldsymbol{\theta})^T\right)$, where $J_g(\boldsymbol{\theta})$ is the Jacobian of g, *i.e.* the $r \times p = 1 \times 3$ matrix of partial derivatives of the entries of g with respect to the entries of $\boldsymbol{\theta}$ and J is defined in equation (13).

For this purpose, considering the Birnbaum-Saunders approximation given in (11), we need to invert the Birnbaum-Saunders CDF and consider $g(\boldsymbol{\theta}) = g_q(\boldsymbol{\theta}) = \mathbb{F}^{-1}_{BS}(q|\boldsymbol{\theta})$ in the DM. The resulting function g is given by the following equation:

$$\begin{aligned} g_q(\boldsymbol{\theta}) &= \left(\Phi[h(P^q_{T_\rho}|\boldsymbol{\theta})]\right)^{-1} = h^{-1}\left(\Phi^{-1}(q)|\boldsymbol{\theta}\right) \\ &= 2^{-1/b}\left(\frac{2c\rho u + 2c\, erf_c^{-1}(2q)^2 - \sqrt{2}c\, erf_c^{-1}(2q)\sqrt{4\rho u + 2\, erf_c^{-1}(2q)^2}}{c^2}\right)^{1/b}, \end{aligned} \tag{19}$$

where $h(t|\boldsymbol{\theta}) = \sqrt{u\rho}\left(\sqrt{\frac{v(t)}{u\rho}} - \sqrt{\frac{u\rho}{v(t)}}\right)$ refers to Birnbaum-Saunders approximation $\mathbb{F}_{BS}(t|\boldsymbol{\theta}) = \Phi\left(h(t|\boldsymbol{\theta})\right)$ in equation (11) and erf_c^{-1} denotes the inverse function of erf_c which is the complementary error function given in the following expression:

$$erf_c(z) = \frac{2}{\sqrt{\pi}}\int_z^\infty exp(-t^2)dt. \tag{20}$$

3.3. Bootstrap techniques

In the previous section, confidence intervals were built upon the assumption of asymptotic convergence of MLE, which implies that the total number of observations is large enough to be considered as infinite: $N = \sum_{j=1}^m n_j \to +\infty$. Because of the small size of data studied in section 4, the CLT conditions may not be satisfied. In this section, we consider using several bootstrap techniques to enrich dataset and analyze the asymptotic confidence bounds. Efron [46] and Efron and Tibshirani [47] were the firsts to introduce the principle of bootstrapping. It consists in drawing in a reference sample to built a large number of bootstrap samples with the same size as the original data (see [48]) and in estimating the model parameters

on each of these samples. Especially, [49] showed this type of techniques is useful to approximate parameters' estimators distributions of complex models from a small number of data.

3.3.1. Parametric bootstrap

For parametric bootstrap (PB), we make the assumption that data come from a given parametric model and the fitted gamma process and its associated parameter $\hat{\boldsymbol{\theta}}_{ML}$ are used to generate new datasets [50, 51]. Given the observations $\mathbf{D}_{obs}$, with size $N = \sum_{j=1}^{m} n_j$, we first estimate $\hat{\boldsymbol{\theta}}_{ML}$ (see section 2.4). Then, $\hat{\boldsymbol{\theta}}_{ML}$ is used to resample B times m degradation paths of length n_j, $1 \leq j \leq m$, of the gamma process using the GSS method [52]. Hence, the resulting B bootstrap samples are used to obtain B estimates of $\hat{\boldsymbol{\theta}}_{ML}$: $\hat{\boldsymbol{\theta}}^*_{PB,v}$, $1 \leq v \leq B$. From these B values of $\hat{\boldsymbol{\theta}}^*_{PB}$, we can derive information on the estimation uncertainty on $\hat{\boldsymbol{\theta}}_{ML}$ and thus on how $\hat{\boldsymbol{\theta}}_{ML}$ behaves in comparison to $\boldsymbol{\theta}$. We can illustrate the procedure with the following algorithm:

1. Given the degradation observations $\mathbf{D}_{obs}$, fit a non-homogeneous gamma process. This leads to MLE $\hat{\boldsymbol{\theta}}_{ML}$.
2. Generate m degradation paths of length n_j, $1 \leq j \leq m$, following the gamma process having $\hat{\boldsymbol{\theta}}_{ML}$ as parameter on discrete time interval $[0, t_{n_j}]$.
3. Estimate $\hat{\boldsymbol{\theta}}^*_{PB}$ from step 2. new dataset.
4. Repeat steps 2. and 3. B times to get B MLE: $\hat{\boldsymbol{\theta}}^*_{PB,v}$, $1 \leq v \leq B$, from B simulated datasets of N measurements.
5. From the B obtained $\hat{\boldsymbol{\theta}}^*_{PB,v}$, $1 \leq v \leq B$, compute the empirical mean $\overline{\hat{\boldsymbol{\theta}}^*_{PB}} = \frac{1}{B}\sum_{v=1}^{B} \hat{\boldsymbol{\theta}}^*_{PB,v}$ and the empirical quantiles of order q, $0 < q < 1$, $\hat{P}^q_{\hat{\boldsymbol{\theta}}^*_{PB}}$. These quantiles give an image of the scatter of $\hat{\boldsymbol{\theta}}^*_{PB}$ compared with $\hat{\boldsymbol{\theta}}_{ML}$ and allow to derive order of magnitude of the statistical estimation uncertainty on $\boldsymbol{\theta}$.

We will consider $\hat{\boldsymbol{\theta}}_{PB}$ is the natural boostrap estimator of $\boldsymbol{\theta}$, with $\hat{\boldsymbol{\theta}}_{PB} = \overline{\hat{\boldsymbol{\theta}}^*_{PB}} = \frac{1}{B}\sum_{v=1}^{B} \hat{\boldsymbol{\theta}}^*_{PB,v}$.

3.3.2. Non-parametric bootstrap

Non-parametric bootstrap techniques consist in resampling data like parametric bootstrap method except that data are not assumed to belong to a given parametric model.

Moving Block Bootstrap (MBB). When data are organized in time series, resampling single observations as considered by Efron and Tibshirani [47] can fail to produce valid approximations in presence of dependence (in time or between components) [53]. Thus, to solve this issue, Moving Block Bootstrap (MBB) can be suitable to efficiently resample time-dependent data such as erosive cavitation successive measurements. This resampling method relies on retaining neighbors observations to form blocks. This way, the dependence structure of data at short distances is preserved, Kreiss and Lahiri [53].

Let us consider the j^{th} degradation path of length n_j of a gamma process as a time series and that degradation increments $\delta_{i,j}$ are observed between discrete times $t_{i,j}$ and $t_{i+1,j}$, $0 \leq i \leq n_j - 1$. We denote $\mathbf{Y}_j = \{Y_{0,j}, \ldots, Y_{n_j-1,j}\}$, with $Y_{i,j} = \{t_{i,j}, t_{i+1,j}, \delta_{i,j}\}$, $1 \leq j \leq m$. Let l be an integer with $1 \leq l \leq n_j$. The overlapping blocks $B_{0,j}, \ldots, B_{p,j}$, $p = n_j - l$ of length l contained in $\mathbf{Y}_j$ are defined as follow:

$$
\begin{aligned}
B_{0,j} &= (Y_{0,j}, Y_{1,j}, \ldots, Y_{l-1,j}),\\
B_{1,j} &= \quad (Y_{1,j}, \ldots, Y_{l-1,j}, Y_{l,j}),\\
&\ldots \qquad\qquad\qquad\qquad \ldots\\
B_{p,j} &= \qquad\qquad\qquad\qquad (Y_{n_j-l,j}, \ldots, Y_{n_j-1,j}).
\end{aligned}
$$

For state of simplicity, consider that n_j is a multiple of l. Let $b_j = n_j/l$. To generate one MBB sample, b_j blocks are taken at random with replacement from the collection $\{B_{0,j}, \ldots, B_{p,j}\}$. The bootstrapped dataset $\mathbf{Y}_j = \{Y^*_{0,j}, \ldots, Y^*_{n_j-1,j}\}$ contains $b_j \cdot l = n_j$ elements since each resampled block has l elements and b_j blocks are drawn. For time-dependent data, l should satisfy the condition: $l = Cn_j^{1/k}$, with $k = 3$ or 4, where $C \in \mathbb{R}$ is a constant [53]. In the general case, where l does not divide n_j, $b_j = b_0$ blocks may be resampled with $b_0 = \min\{k \geq 1 : kl \geq n_j\}$ and only the first n_j resampled data-values are retained to define the bootstrap observations $\mathbf{Y}^*_j$. The following algorithm illustrates the MBB procedure:

1. Set the block length l.
2. Draw with replacement a block of l consecutive observations from $\mathbf{Y}_j$.
3. Repeat b_j times step 2. until the bootstrap sample $\mathbf{Y}^*_j$ has $b_j \cdot l \geq n_j$ elements.
4. Retain only the first n_j resampled values.
5. Repeat steps 2-4 for each degradation path j, $1 \leq j \leq m$, to get a set of m paths $\mathbf{Y}^* = \{\mathbf{Y}^*_1, \ldots, \mathbf{Y}^*_m\}$.
6. Repeat steps 5. B times to generate B sets of bootstrap samples $\mathbf{Y}^*_v$, $1 \leq v \leq B$.
7. Compute $\hat{\boldsymbol{\theta}}^*_{MBB,v}$ using the ML method for each bootstrap samples $\mathbf{Y}^*_v$.

Similarly to PB method, from the B obtained $\hat{\boldsymbol{\theta}}^*_{MBB,v}$, $1 \leq v \leq B$, we can consider $\hat{\boldsymbol{\theta}}_{MBB} = \overline{\hat{\boldsymbol{\theta}}^*_{MBB}} = \frac{1}{B}\sum_{v=1}^{B} \hat{\boldsymbol{\theta}}^*_{MBB,v}$ the natural MBB estimate of $\boldsymbol{\theta}$, and the empirical quantiles of order q, $0 < q < 1$, $\hat{P}^q_{\hat{\boldsymbol{\theta}}^*_{MBB}}$. In the case study presented in the next section, the block length l was chosen equal to 3 to make a compromise between time dependence structure and the relative short path length n_j.

Efron bootstrap (EB). The bootstrap method originally introduced by Efron [46] can be seen as a special case of MBB. Indeed if we set $l = 1$, the MBB is equivalent to the ordinary non parametric bootstrap method described by Efron and Tibshirani [47] for i.i.d. data. Similarly to previous methods, from the B obtained $\hat{\boldsymbol{\theta}}^*_{EB,v}$, $1 \leq v \leq B$, we can introduce the empirical mean $\hat{\boldsymbol{\theta}}_{EB} = \overline{\hat{\boldsymbol{\theta}}^*_{EB}} = \frac{1}{B}\sum_{v=1}^{B} \hat{\boldsymbol{\theta}}^*_{EB,v}$ which will be considered as the EB estimate of $\boldsymbol{\theta}$, and the empirical quantiles of order q, $0 < q < 1$, $\hat{P}^q_{\hat{\boldsymbol{\theta}}^*_{EB}}$.

3.3.3. Bootstrap uncertainty on hitting time T_ρ

From the B obtained $\hat{\boldsymbol{\theta}}_v^*$, $1 \leq v \leq B$, from previous bootstrap techniques, the percentiles (of order q) of first hitting time distribution, noted $\mathbb{F}_{BS}^{-1}(q|\hat{\boldsymbol{\theta}}_v^*)$, can be easily derived using the Birnbaum-Saunders approximation (see section 3.2).

3.4. Statistical indicators for performance assessment

In Table 1, we introduce some classic statistical indicators to assess bootstrap techniques performance and compare them with MLE + DM. If we consider the case of model parameters' estimation, bias measures how well the true unknown parameter $\boldsymbol{\theta}$ is approximated by $\hat{\boldsymbol{\theta}}$. Similarly, variance and dispersion give an indication on the estimation accuracy of $\boldsymbol{\theta}$ by $\hat{\boldsymbol{\theta}}$. Finally, the Mean Squared Error (MSE) combines both indicators and allows to compare techniques between each other. $\overline{\hat{\boldsymbol{\theta}}^*}$ denotes the mean of $\hat{\boldsymbol{\theta}}_v^*$, $1 \leq v \leq B$, as introduced for each bootstrap technique in the previous sections.

	Mathematical expression
Bias	$\overline{\hat{\boldsymbol{\theta}}^*} - \hat{\boldsymbol{\theta}}_{ML}$
Relative bias	$\dfrac{\overline{\hat{\boldsymbol{\theta}}^*} - \hat{\boldsymbol{\theta}}_{ML}}{\hat{\boldsymbol{\theta}}_{ML}}$
Variance	$\dfrac{1}{B}\sum_{v=1}^{B}\left(\hat{\boldsymbol{\theta}}_v^* - \overline{\hat{\boldsymbol{\theta}}^*}\right)^2$
Relative error	$\dfrac{\sqrt{\text{variance}}}{\overline{\hat{\boldsymbol{\theta}}^*}}$
Dispersion (at 95%)	$\hat{P}_{\hat{\boldsymbol{\theta}}^*}^{97.5\%} - \hat{P}_{\hat{\boldsymbol{\theta}}^*}^{2.5\%}$
Mean squared error	bias^2 + variance

Table 1: Statistical indicators used to assess bootstrap methods performance

4. Case study

4.1. Experimental dataset

In this study, we aim to model erosive cavitation using NHGP and evaluate confidence intervals of model parameters with limited dataset. In [54], a sensitivity analysis was conducted on gamma process parameters and size of dataset using *Monte Carlo* simulations. The latter study shows the performances of maximum likelihood estimation vary depending on the degradation acceleration (parameter b of the shape function)

and the number of paths m. In particular, authors show a dataset with more degradation paths should be preferred for a same total number of observations N.

Although we focused in the present paper on modeling cavitation observed on hydraulic runner, the same methodology can be applied to other cumulative and monotonic deterioration measured on other types of systems. Moreover, resulting hitting time distribution variability will be computed according to the results from the previous confidence intervals (using DM and bootstrap techniques). We used a dataset $\mathbf{D}_{obs}$ consisting in $m = 3$ degradation paths presented in Figure 3 (right) obtained from a vibratory cavitation test (2 replications) performed in laboratory conforming to standard given in [55]. During test j, the degradation level, here the specimen mass, is measured at instants $t_{i,j}$, $1 \leq i \leq n_j$, to determine the cumulative mass loss $x_{i,j}$ as depicted by degradation path j in Figure 1. Meanwhile, for actual Francis turbine prototypes, the incubation and acceleration regions of the erosive cavitation pattern (shown in Figure 3 (left)) are not observed. For this reason, we decided to only focus on modeling the degradation on the maximum rate region (*ie*: from time $= t_{A,j}$ to t_{n_j}). First, degradation data in the region of interest have been transformed to satisfy the first gamma process property, $X(0) = 0$, with $t'_{i,j} = t_{i,j} - t_{A,j}$ and $x'_{i,j} = x_{i,j} - x_{A,j}, A \leq i \leq n_j$. Note that $t_{A,j}$ (considered to be deterministic) is determined by the intersection between the x-axis and the slope of the degradation path in the maximum stage region. Further explanations on the standard test method can be found, as detailed in [55]. Because we notice in Figure 3 (right) an increasing trend in degradation over time, we chose to model it with a NHGP (a performance comparison, conducted previously in [56] on the same dataset, between homogeneous and non-homogeneous gamma process has shown better results for NHGP). Thus, $\hat{\boldsymbol{\theta}}_{ML} = (\hat{u}_{ML}, \hat{c}_{ML}, \hat{b}_{ML})$ was computed from the $m = 3$ paths of length $n_j \in \{10, 10, 14\}$, $1 \leq j \leq 3$, for a total of $N = \sum_{j=1}^{m=3} n_j = 34$ observations, using ML equations (see section 2.4) and optimization tools. Because of numerical difficulties induced by the gamma function, equations (5) to (7) have been used instead of maximizing directly expression (4).

4.2. Calibration of bootstrap sample number

In order to determine a relevant value of B, the number of bootstrap datasets to be drawn (see section 3.3.2), a convergence analysis was performed. For this purpose, we considered the previous dataset $\mathbf{D}_{obs}$ and the three bootstrap methods were applied for different values of B, $10 \leq B \leq 10^4$. Figure 4 shows $\hat{\boldsymbol{\theta}}_{EB}$ and percentiles, $\hat{P}^{2.5\%}_{\hat{\boldsymbol{\theta}}^*_{EB}}$ and $\hat{P}^{97.5\%}_{\hat{\boldsymbol{\theta}}^*_{EB}}$, respectively represented with upper and lower bars as defined in Section 3.3. We observe the asymptotic convergence is reached around $B = 10^3$ draws. We retained $B = 10^4$ draws for the three bootstrap techniques to ensure a good convergence.

4.3. Estimation uncertainties for model parameters

The three different boostrap methods presented in section 3.3 have been applied on the experimental dataset introduced in section 4.1. Approximate asymptotic confidence intervals introduced in section 3.3.1 were derived to get the approximate symmetrical two-sided 95% confidence intervals on $\boldsymbol{\theta}$.

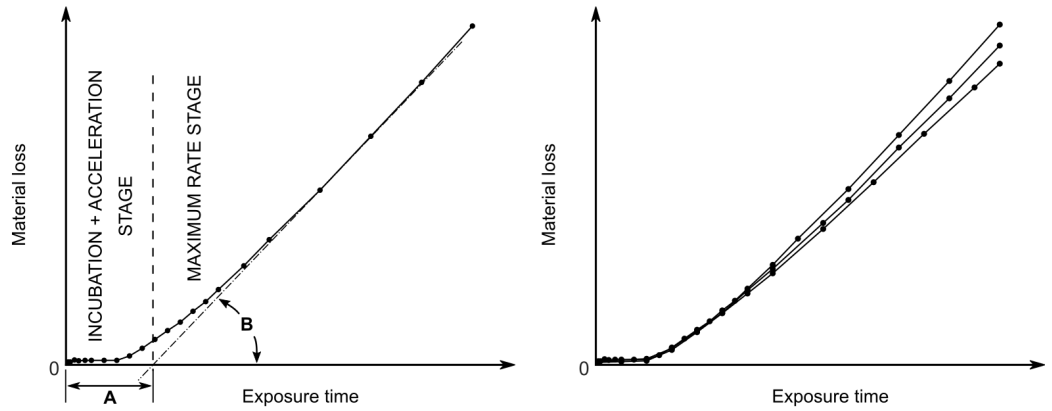

Figure 3: (Left) Characteristic stages of the cumulative erosion-time curve, adapted from [55] - (Right) Cavitation erosion paths ($m = 3$) from laboratory.

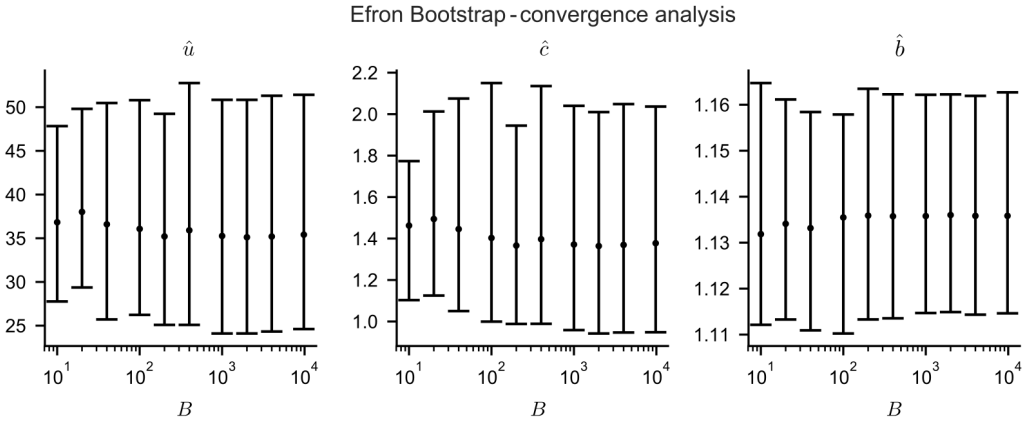

Figure 4: $\hat{\boldsymbol{\theta}}_{EB}$, $\hat{P}^{2.5\%}_{\hat{\boldsymbol{\theta}}^*_{EB}}$ and $\hat{P}^{97.5\%}_{\hat{\boldsymbol{\theta}}^*_{EB}}$ - Convergence analysis on bootstrap iteration number B for EB method

Table 3 presents statistical indicators from bootstrap techniques and ML results. For ML method, results are derived from formulas (12) and (16). We observed in this study, that the best methods (EB and MBB), with the relative error reaching around 25% for parameters u and c, which can be considered as quite high. Meanwhile, EB seems to produce better estimation of $\boldsymbol{\theta}$ than MBB in terms of relative estimation uncertainties. For better illustration and comparison, Figure 5 shows boxplots of $\hat{\boldsymbol{\theta}}^*_v$, $1 \leq v \leq B$, for the three bootstrap techniques. Lower and upper whiskers denote $\hat{P}^{2.5\%}_{\hat{\boldsymbol{\theta}}^*}$ and $\hat{P}^{97.5\%}_{\hat{\boldsymbol{\theta}}^*}$ respectively; box shows first $\hat{P}^{25\%}_{\hat{\boldsymbol{\theta}}^*}$ and third $\hat{P}^{75\%}_{\hat{\boldsymbol{\theta}}^*}$ quartiles and median $\hat{P}^{50\%}_{\hat{\boldsymbol{\theta}}^*}$. Left and right doted lines respectively represent the lower and upper bounds of the asymptotic two-sided 95% confidence intervals in Table 2, obtained by the asymptotic normality of MLE. The centered doted line represents $\hat{\boldsymbol{\theta}}_{ML} = (\hat{u}_{ML}, \hat{c}_{ML}, \hat{b}_{ML})$. In both Table 3

	$\hat{u}$	$\hat{c}$	$\hat{b}$
ML	32.501	1.2722	1.1348
Approximate asymptotic CI (at 95%)	[16.32, 48.69]	[1.101, 1.939]	[1.108, 1.162]
PB	35.154	1.9516	1.0888
EB	34.971	1.3572	1.1361
MBB	36.420	1.3549	1.1421

Table 2: Estimations of $\boldsymbol{\theta}$ for ML method and 3 different bootstrap techniques - Approximate asymptotic confidence interval (at 95%) of $\boldsymbol{\theta}$.

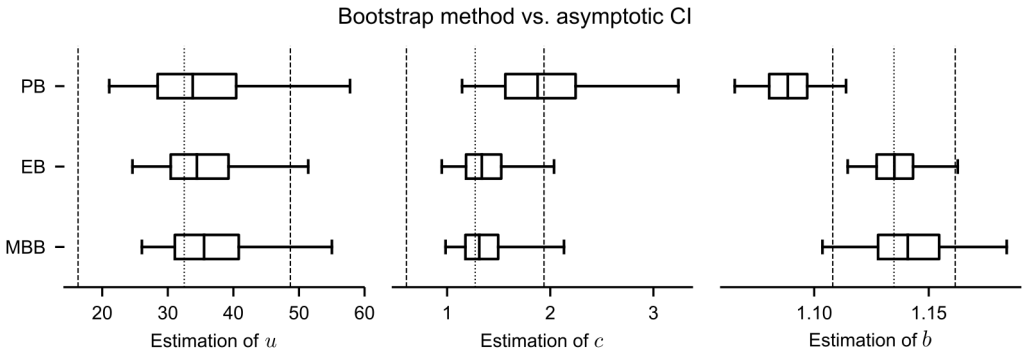

Figure 5: Comparison of bootstrap and asymptotic CI.

and Figure 5 we observe the largest (positive, leading to a possible over-estimation) bias (but also relative bias) for PB method (for parameters c and b, around 10% and 50% respectively) and the largest scatter on u and c, while EB and MBB bias is around 10%. In terms of bias and scatter, EB and MBB show similar results except for EB estimation of b which exhibits a bias close to zero. One of the main hypothesis of approximate asymptotic confidence intervals from MLE is highlighted in Table 3: $\hat{\boldsymbol{\theta}}_{ML}$ is considered centered on true unknown parameter $\boldsymbol{\theta}$ and hence shows no bias (asymptotically, which may be a wrong hypothesis for small dataset). Nonetheless, considering ML has no bias, the MSE is the smallest for EB method on both u, b and c parameters. We observe in Figure 5 boxplots are asymmetrical while approximate asymptotic CI are centered around $\hat{\boldsymbol{\theta}}_{ML}$ which is not confirmed by bootstrap distributions of $\hat{\boldsymbol{\theta}}^*$. Tables 2, 3 and Figure 5 show a small relative error on parameter b estimations (around 1%) for non-parametric methods and exhibit value of power $b = 1$ is not included in confidence interval at 95% level, thus justifying the use of NHGP to model our cavitation erosion dataset.

		ML	Bootstrap techniques		
			PB	EB	MBB
Bias	$\hat{u}$	0 (supposed)	2.653	2.470	3.919
	$\hat{c}$		0.6794	0.0850	0.0827
	$\hat{b}$		-0.0461	0.0013	0.0073
Relative bias	$\hat{u}$	0 (supposed)	0.0816	0.0760	0.1206
	$\hat{c}$		0.5340	0.0668	0.0650
	$\hat{b}$		-0.0406	0.0011	0.0064
Variance	$\hat{u}$	68.20	87.56	48.59	58.11
	$\hat{c}$	0.1158	0.2926	0.0787	0.0865
	$\hat{b}$	0.0002	0.0002	0.0002	0.0004
Relative error	$\hat{u}$	0.2541	0.2879	0.2145	0.2346
	$\hat{c}$	0.2675	0.4252	0.2206	0.2312
	$\hat{b}$	0.0120	0.0109	0.0108	0.0182
Dispersion at 95%	$\hat{u}$	32.64	36.77	25.84	29.31
	$\hat{c}$	0.838	2.099	1.040	1.133
	$\hat{b}$	0.0540	0.0486	0.0485	0.0814
MSE	$\hat{u}$	68.195	94.69	56.74	73.89
	$\hat{c}$	0.1158	0.7544	0.08961	0.09553
	$\hat{b}$	0.0002	0.0023	0.0002	0.0003

Table 3: Statistical indicators from different methods' results

Quartiles of T_ρ		ML+DM	PB	EB	MBB
$P_{T_\rho}^{2.5\%}$	Median	976	950	976	976
	Dispersion at 95%	31	40	40	54
	Relative error	0.032	0.042	0.041	0.055
$P_{T_\rho}^{50\%}$	Median	1006	979	1005	1006
	Dispersion at 95%	31	40	40	54
	Relative error	0.031	0.041	0.040	0.054
$P_{T_\rho}^{97.5\%}$	Median	1037	1011	1036	1036
	Dispersion at 95%	34	44	41	56
	Relative error	0.033	0.044	0.040	0.054

Table 4: Estimation of hitting time percentiles: $P_{T_\rho}^{2.5\%}$, $P_{T_\rho}^{50\%}$, $P_{T_\rho}^{97.5\%}$ and their associated estimation uncertainty for the 3 bootstrap methods and ML + DM.

4.4. Influence of model parameter uncertainties on hitting-time

Figure 6 illustrates the concept of propagation of uncertainties. Indeed, influence of $\boldsymbol{\theta}$ estimation uncertainty on hitting time distributions $\mathbb{F}_{T_\rho}$ can be derived using the Birnbaum-Saunders approximation from both delta method (see section 3.2) and bootstrap techniques results. To study how uncertainties impact the whole distribution of T_ρ (threshold $\rho = 100\ mg$), we compute in Figure 6 for each percentile order $q = \{2.5\%, 5\%, \ldots, 97.5\%\}$: $\mathbb{F}_{BS}^{-1}(q|\hat{\boldsymbol{\theta}}_{ML})$ and its variability using DM (see section 3.2) and $\mathbb{F}_{BS}^{-1}(q|\hat{\boldsymbol{\theta}}_v^*)$, with $1 \leq v \leq B$, for the three bootstrap techniques (see section 3.3). In Figure 6, doted lines and shaded areas represent respectively medians and $\hat{P}_{P_{T_\rho}^q}^{75\%} - \hat{P}_{P_{T_\rho}^q}^{25\%}$ of $\mathbb{F}_{BS}^{-1}(q|\hat{\boldsymbol{\theta}}_v^*)$. We observe clearly that the dispersion seems to remain constant for the different percentile orders q for all bootstrap methods. As observed in Figure 5 with boxplots, the shaded areas in Figure 6 are slightly asymmetrical compared to median (more significantly for MBB technique): most values are concentrated on lower half of distribution. ML+DM, EB and MBB produce very close results on both percentiles of lower and upper orders but also on percentile estimation of central order. For ML+DM and EB methods, we observe also close results in terms of dispersion of percentile estimations. Only MBB produces larger dispersion on hitting time percentile distributions. If we look closely at the relative error of $P_{T_\rho}^q$ in Table 4, we can stress that T_ρ seems to be better estimated than $\boldsymbol{\theta}$. This result could be explained by an offset effect of estimation uncertainty of parameters u, c and b on the hitting time distribution.

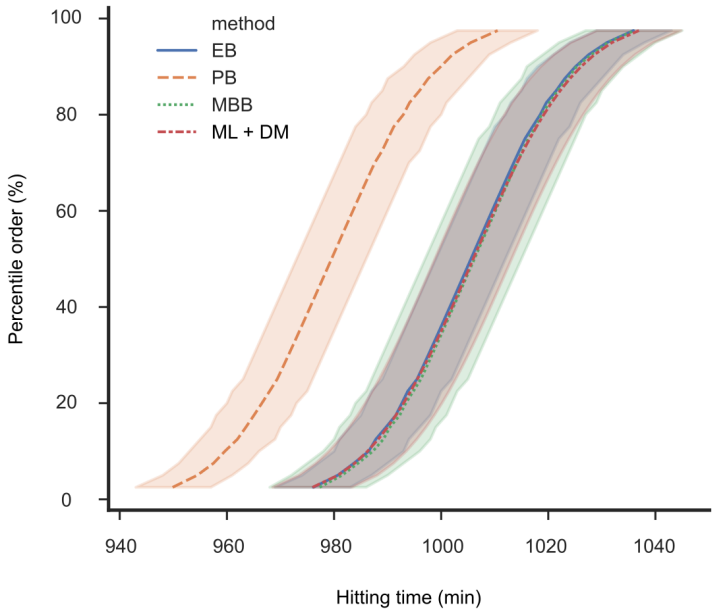

Figure 6: Hitting time distributions of T_ρ (for $\rho = 100\ mg$) for 3 bootstrap methods and ML + DM.

5. Discussion

In the light of results presented in section 4.3, the use of a NHGP can be justified considering CI of parameter b does not include value 1, *i.e.* the homogeneous case. Non-parametric bootstrap techniques seem to provide results close to ML method, while parametric bootstrap presents both the largest bias and scatter on parameter estimation. Even if this may seem counter-intuitive, we noticed PB tends to fail producing "good" simulated paths when their length n_j is small (lower than 10^3 increments). This trend is particularly true for NHGP, with a MLE convergence performance worse than HGP for short path length.

MBB and EB give a good estimation of the degradation acceleration depicted by power parameter b, with relative bias and dispersion lower than 1% for both methods. The same indicator reaches around 10% for parameters u and c, which denotes that non parametric bootstrap methods have more difficulties when it comes to estimate these parameters. Among bootstrap techniques, EB seems to produce the closest estimations relatively to $\hat{\boldsymbol{\theta}}_{ML}$. This result can be surprising considering MBB is supposed to better capture temporal dependence of time series. This may be explained by the relatively small dataset (short path length) used to resample; the new resampled dataset does not provide much more information compared to the original one. Note that this remark applies also for other bootstrap techniques.

According to Table 3 and Figure 6, we observe that the estimation uncertainty on parameter b has the greatest influence on hitting time distribution. The larger the scatter on parameter b is, the larger T_ρ percentile estimate scatter at a given order will be. A further investigation should be carried out to

quantify the influence of each parameter on hitting time T_ρ using a sensitivity analysis. Combination of ML and DM seems to give results close to EB, for a computing lower cost: around 0.0029 sec [1] for ML+DM and around 2035 sec for bootstrap techniques (to generate $B = 10^4$ datasets and estimate the associated parameters). Meanwhile, mathematical developments require much more effort for the DM to obtain uncertainty on hitting time distribution. Moreover, bootstrap techniques give the entire distribution of parameters' estimators instead of only brackets centered on $\hat{\boldsymbol{\theta}}_{ML}$ for approximate asymptotic confidence intervals for ML method. This feature allows, in the case of bootstrap techniques, to estimate possible bias between $\hat{\boldsymbol{\theta}}_{ML}$ and $\boldsymbol{\theta}$. For these reasons and because ML relies on asymptotic hypothesis (not necessarily satisfied), EB shows better performances and tends to be more robust than the combination of ML and DM.

6. Conclusion and perspectives

In this paper we modeled erosive cavitation from laboratory experiments with a stochastic process taking into account physical random dynamics. Maximum likelihood method was used to estimate the unknown parameters of the NHGP. Moreover, several methods were used to assess model parameters estimation uncertainties and their influence on the distribution of the hitting time for a given degradation level threshold. To our knowledge, we are the first to apply delta method in the framework of gamma processes. It is found on our case that the combination of ML+DM, and Efron bootstrap produce similar results. Meanwhile, bootstrap methods exhibit quicker and simpler implementation than delta method. Similarly, MBB shows a reasonable bias but more dispersion. On the contrary, PB fails to give "accurate" estimates of parameters. However, reader needs to keep in mind the reference dataset show a particularly small size and general conclusions should not be drawn from this specific case. In particular, data were collected during experiments under controlled environment showing small discrepancy. Meanwhile, random effect models can be useful to consider unexplained heterogeneous degradation rates within a same product population or a same test procedure [23, 57]. For a further study on the performances of ML parameter estimation, we refer the reader to [54].

Because of the small dataset and the potential availability of other sources of information about cavitation erosion, such as expert knowledge, monitoring data or results from numerical simulations, a Bayesian framework should be well suited to combine these multiple sources of information and decrease uncertainty on parameters estimations [58, 59]. Further investigation could be carried out using other stochastic processes or degradation models such as degradation paths [11], cumulative shock models [30] or inverse gaussian process [23]. Likewise, other bootstrap techniques, such as Markov bootstrap [60], could also be investigated.

This paper can be seen as the first step in development of condition based maintenance policies for high cost systems as presented in [61] and Lei et al. [62]. Although this study focuses on cavitation erosion, a

[1] performed on a quad core Intel i7 2.8GHz processor with 16GB RAM

similar methodology could be applied to other cumulative and monotonic degradation observed on different systems. Next steps would imply using real monitoring cavitation measurements and study the influence on degradation phenomenon of covariates, such as material properties of studied systems or even operating conditions, to develop specific sub-models. These improvements may lead to more realistic degradation prediction and maintenance planning.

Appendix A.

For a gamma process with shape function $v(t) = ct^b$, first and second partial derivatives of log-likelihood function $\ell(\boldsymbol{\theta})$, respectively to parameter $\boldsymbol{\theta}$, are given in the following expressions:

$$\begin{aligned}
\frac{\partial \ell(\boldsymbol{\theta})}{\partial u} &= \sum_{j=1}^{m}\sum_{i=1}^{n_j} \tfrac{c}{u}\left[t_{i,j}^b - t_{i-1,j}^b\right] - \delta_{i,j} \\
\frac{\partial \ell(\boldsymbol{\theta})}{\partial c} &= \sum_{j=1}^{m}\sum_{i=1}^{n_j} \left[t_{i,j}^b - t_{i-1,j}^b\right]\left[\log(\delta_{i,j}) + \log(u) - \psi\left(c[t_{i,j}^b - t_{i-1,j}^b]\right)\right] \\
\frac{\partial \ell(\boldsymbol{\theta})}{\partial b} &= \sum_{j=1}^{m}\sum_{i=1}^{n_j} c\left[t_{i,j}^b \log(t_{i,j}) - t_{i-1,j}^b \log(t_{i-1,j})\right]\left[\log(\delta_{i,j}) - \psi\left(c[t_{i,j}^b - t_{i-1,j}^b]\right) + \log(u)\right]
\end{aligned} \tag{A.1}$$

$$\begin{aligned}
\frac{\partial^2 \ell(\boldsymbol{\theta})}{\partial u^2} &= -\sum_{j=1}^{m}\sum_{i=1}^{n_j} \tfrac{c}{u^2}\left[t_{i,j}^b - t_{i-1,j}^b\right] \\
\frac{\partial^2 \ell(\boldsymbol{\theta})}{\partial c^2} &= -\sum_{j=1}^{m}\sum_{i=1}^{n_j} \left[t_{i,j}^b - t_{i-1,j}^b\right]^2 \psi'\left(c[t_{i,j}^b - t_{i-1,j}^b]\right) \\
\frac{\partial^2 \ell(\boldsymbol{\theta})}{\partial b^2} &= \sum_{j=1}^{m}\sum_{i=1}^{n_j} c\left\{\left[t_{i,j}^b \log(t_{i,j})^2 - t_{i-1,j}^b \log(t_{i-1,j})^2\right]\left[\log(t_{i,j}) - \psi(c[t_{i,j}^b - t_{i-1,j}^b]) + \log(u)\right]\right. \\
&\quad \left. -c\left[t_{i,j}^b \log(t_{i,j}) - t_{i-1,j}^b \log(t_{i-1,j})\right]^2\left[\psi'\left(c[t_{i,j}^b - t_{i-1,j}^b]\right)\right]\right\} \\
\frac{\partial^2 \ell(\boldsymbol{\theta})}{\partial u \partial c} &= \sum_{j=1}^{m}\sum_{i=1}^{n_j} \tfrac{1}{c}\left[t_{i,j}^b - t_{i-1,j}^b\right] \\
\frac{\partial^2 \ell(\boldsymbol{\theta})}{\partial u \partial b} &= \sum_{j=1}^{m}\sum_{i=1}^{n_j} \tfrac{c}{v}\left[t_{i,j}^b \log(t_{i,j}) - t_{i-1,j}^b \log(t_{i-1,j})\right] \\
\frac{\partial^2 \ell(\boldsymbol{\theta})}{\partial c \partial u} &= \sum_{j=1}^{m}\sum_{i=1}^{n_j} \tfrac{1}{u}\left[t_{i,j}^b - t_{i-1,j}^b\right] \\
\frac{\partial^2 \ell(\boldsymbol{\theta})}{\partial c \partial b} &= \sum_{j=1}^{m}\sum_{i=1}^{n_j} \left[t_{i,j}^b \log(t_{i,j}) - t_{i-1,j}^b \log(t_{i-1,j})\right]\left\{\log(\delta_{i,j} - \psi\left(c[t_{i,j}^b - t_{i-1,j}^b]\right) + \log(u)\right. \\
&\quad \left. -c[t_{i,j}^b - t_{i-1,j}^b]\psi'\left(c[t_{i,j}^b - t_{i-1,j}^b]\right)\right\} \\
\frac{\partial^2 \ell(\boldsymbol{\theta})}{\partial b \partial u} &= \frac{\partial^2 \ell(\boldsymbol{\theta})}{\partial u \partial b} \\
\frac{\partial^2 \ell(\boldsymbol{\theta})}{\partial b \partial c} &= \frac{\partial^2 \ell(\boldsymbol{\theta})}{\partial c \partial b}
\end{aligned} \tag{A.2}$$

References

[1] K. T. Nguyen, M. Fouladirad, A. Grall, Model selection for degradation modeling and prognosis with health monitoring data, Reliability Engineering & System Safety 169 (2018) 105–116.

[2] A. K. Verma, S. Ajit, D. R. Karanki, Reliability and safety engineering, volume 43, Springer, 2010.

[3] W. Kahle, S. Mercier, C. Paroissin, Degradation processes in reliability, John Wiley & Sons, 2016.

[4] X. Escaler, E. Egusquiza, M. Farhat, F. Avellan, M. Coussirat, Detection of cavitation in hydraulic turbines, Mechanical systems and signal processing 20 (2006) 983–1007.

[5] C. E. Brennen, Cavitation and bubble dynamics, Cambridge University Press, 2013.

[6] K. Celebioglu, B. Altintas, S. Aradag, Y. Tascioglu, Numerical research of cavitation on francis turbine runners, International Journal of Hydrogen Energy 42 (2017) 17771–17781.

[7] L. Krumenacker, R. Fortes-Patella, A. Archer, Numerical estimation of cavitation intensity, in: IOP Conference Series: Earth and Environmental Science, volume 22, IOP Publishing, 2014.

[8] P. Gohil, R. Saini, Numerical study of cavitation in francis turbine of a small hydro power plant, Journal of Applied Fluid Mechanics 9 (2016).

[9] N. D. Singpurwalla, Survival in dynamic environments, Statistical science (1995) 86–103.

[10] E. A. Elsayed, Reliability engineering, John Wiley & Sons, 2020.

[11] Z. Xu, Y. Hong, R. Jin, Nonlinear general path models for degradation data with dynamic covariates, Applied Stochastic Models in Business and Industry 32 (2016) 153–167.

[12] J. Van Noortwijk, A survey of the application of gamma processes in maintenance, Reliability Engineering & System Safety 94 (2009) 2–21.

[13] S. Alaswad, Y. Xiang, A review on condition-based maintenance optimization models for stochastically deteriorating system, Reliability Engineering & System Safety 157 (2017) 54–63.

[14] C. M. Grinstead, J. L. Snell, Introduction to probability, American Mathematical Soc., 2012.

[15] S. Karlin, A first course in stochastic processes, Academic press, 2014.

[16] S. Kadloor, R. S. Adve, A. W. Eckford, Molecular communication using brownian motion with drift, IEEE Transactions on NanoBioscience 11 (2012) 89–99.

[17] Z. Zhang, X. Si, C. Hu, Y. Lei, Degradation data analysis and remaining useful life estimation: A review on wiener-process-based methods, European Journal of Operational Research (2018).

[18] E. Çınlar, Probability and stochastics, volume 261, Springer Science & Business Media, 2011.

[19] X. Wang, D. Xu, An inverse gaussian process model for degradation data, Technometrics 52 (2010) 188–197.

[20] M. Abdel-Hameed, A gamma wear process, IEEE transactions on Reliability 24 (1975) 152–153.

[21] Q. Guan, Y. Tang, A. Xu, Objective bayesian analysis accelerated degradation test based on wiener process models, Applied Mathematical Modelling 40 (2016) 2743–2755.

[22] G. Whitmore, Estimating degradation by a wiener diffusion process subject to measurement error, Lifetime data analysis 1 (1995) 307–319.

[23] C.-Y. Peng, Inverse gaussian processes with random effects and explanatory variables for degradation data, Technometrics 57 (2015) 100–111.

[24] M. H. Ling, K. L. Tsui, N. Balakrishnan, Accelerated degradation analysis for the quality of a system based on the gamma process, IEEE Transactions on Reliability 64 (2015) 463–472.

[25] Z.-S. Ye, N. Chen, The inverse gaussian process as a degradation model, Technometrics 56 (2014) 302–311.

[26] Y. Deng, A. Barros, A. Grall, Degradation modeling based on a time-dependent ornstein-uhlenbeck process and residual useful lifetime estimation, IEEE Transactions on Reliability 65 (2016) 126–140.

[27] B. Castanier, A. Grall, C. Bérenguer, A condition-based maintenance policy with non-periodic inspections for a two-unit series system, Reliability Engineering & System Safety 87 (2005) 109–120.

[28] B. de Jonge, Maintenance Optimization based on Mathematical Modeling, University of Groningen, 2017.

[29] E. Deloux, M. Fouladirad, C. Bérenguer, Health-and-usage-based maintenance policies for a partially observable deteriorating system, Proceedings of the Institution of Mechanical Engineers, Part O: Journal of Risk and Reliability 230 (2016) 120–129.

[30] W. Zhu, M. Fouladirad, C. Bérenguer, Condition-based maintenance policies for a combined wear and shock deterioration model with covariates, Computers & Industrial Engineering 85 (2015) 268–283.

[31] X. Wang, A pseudo-likelihood estimation method for nonhomogeneous gamma process model with random effects, Statistica Sinica 18 (2008) 1153–1163.

[32] K. Le Son, M. Fouladirad, A. Barros, Remaining useful lifetime estimation and noisy gamma deterioration process, Reliability Engineering & System Safety 149 (2016) 76–87.

[33] D. Lu, M. D. Pandey, W.-C. Xie, An efficient method for the estimation of parameters of stochastic gamma process from noisy degradation measurements, Proceedings of the Institution of Mechanical Engineers, Part O: Journal of Risk and Reliability 227 (2013) 425–433.

[34] M. E. Cholette, H. Yu, P. Borghesani, L. Ma, G. Kent, Degradation modeling and condition-based maintenance of boiler heat exchangers using gamma processes, Reliability Engineering & System Safety 183 (2019) 184–196.

[35] B. H. Nystad, G. Gola, J. E. Hulsund, D. Roverso, Technical condition assessment and remaining useful life estimation of choke valves subject to erosion, in: Annual Conference of the Prognostics and Health Management Society, 2010, pp. 11–13.

[36] G. Arfken, The incomplete gamma function and related functions, Mathematical Methods for Physicists (1985) 565–572.

[37] C. Park, W. Padgett, Accelerated degradation models for failure based on geometric brownian motion and gamma processes, Lifetime Data Analysis 11 (2005) 511–527.

[38] C. Paroissin, A. Salami, Failure time of non homogeneous gamma process, Communications in Statistics-Theory and Methods 43 (2014) 3148–3161.

[39] N. Balakrishnan, D. Kundu, Birnbaum-saunders distribution: A review of models, analysis and applications, arXiv preprint arXiv:1805.06730 (2018).

[40] A. Birolini, Reliability engineering, volume 5, Springer, 2007.

[41] B. Hoadley, Asymptotic properties of maximum likelihood estimators for the independent not identically distributed case, The Annals of mathematical statistics (1971) 1977–1991.

[42] C. R. Rao, Linear statistical inference and its applications, volume 2, Wiley New York, 1973.

[43] B. Efron, D. V. Hinkley, Assessing the accuracy of the maximum likelihood estimator: Observed versus expected fisher information, Biometrika 65 (1978) 457–483.

[44] G. Casella, R. L. Berger, Statistical inference, volume 2, Duxbury Pacific Grove, CA, 2002.

[45] M. Fouladirad, C. Paroissin, A. Grall, Sensitivity of optimal replacement policies to lifetime parameter estimates, European Journal of Operational Research 266 (2018) 963–975.

[46] B. Efron, Bootstrap methods: another look at the jackknife, in: Breakthroughs in statistics, Springer, 1992, pp. 569–593.

[47] B. Efron, R. J. Tibshirani, An introduction to the bootstrap, CRC press, 1994.

[48] E. Vittinghoff, D. V. Glidden, S. C. Shiboski, C. E. McCulloch, Regression methods in biostatistics: linear, logistic, survival, and repeated measures models, Springer Science & Business Media, 2011.

[49] T. Kaneishi, T. Dohi, Parametric bootstrapping for assessing software reliability measures, in: Dependable Computing (PRDC), 2011 IEEE 17th Pacific Rim International Symposium on, IEEE, 2011, pp. 1–9.

[50] W. Stute, W. G. Manteiga, M. P. Quindimil, Bootstrap based goodness-of-fit-tests, Metrika 40 (1993) 243–256.

[51] C. Genest, B. Rémillard, et al., Validity of the parametric bootstrap for goodness-of-fit testing in semiparametric models, in: Annales de l'Institut Henri Poincaré, Probabilités et Statistiques, volume 44, Institut Henri Poincaré, 2008, pp. 1096–1127.

[52] A. Avramidis, P. L'ecuyer, P.-A. Tremblay, Efficient simulation of gamma and variance-gamma processes, in: Proceedings of the 2003 Winter Simulation Conference, volume 1, 2003, pp. 319–326.

[53] J.-P. Kreiss, S. N. Lahiri, Bootstrap methods for time series, in: Handbook of statistics, volume 30, Elsevier, 2012, pp.

3–26.

[54] Q. Chatenet, M. Fouladirad, E. Remy, M. Gagnon, L. Ton-That, A. Tahan, On the performance of the maximum likelihood estimation method for gamma process, in: European Safety and Reliability Conference, volume 25, 2019.

[55] Standard Test Method for Cavitation Erosion Using Vibratory Apparatus, Standard, ASTM International, West Conshohocken, PA, 2016. URL: www.astm.org.

[56] Q. Chatenet, M. Gagnon, L. Tôn-Thât, E. Remy, M. Fouladirad, A. Tahan, Stochastic modeling of cavitation erosion in francis runner, International Journal of Fluid Machinery and Systems 13 (2020) 400–408.

[57] Q. Zhai, P. Chen, L. Hong, L. Shen, A random-effects wiener degradation model based on accelerated failure time, Reliability Engineering & System Safety 180 (2018) 94–103.

[58] J. M. Bernardo, A. F. Smith, Bayesian theory, volume 405, John Wiley & Sons, 2009.

[59] N. Bousquet, M. Fouladirad, A. Grall, C. Paroissin, Bayesian gamma processes for optimizing condition-based maintenance under uncertainty, Applied Stochastic Models in Business and Industry 31 (2015) 360–379.

[60] W. Härdle, J. Horowitz, J.-P. Kreiss, Bootstrap methods for time series, International Statistical Review 71 (2003) 435–459.

[61] Q. Zhu, H. Peng, G.-J. van Houtum, A condition-based maintenance policy for multi-component systems with a high maintenance setup cost, Or Spectrum 37 (2015) 1007–1035.

[62] Y. Lei, N. Li, L. Guo, N. Li, T. Yan, J. Lin, Machinery health prognostics: A systematic review from data acquisition to rul prediction, Mechanical Systems and Signal Processing 104 (2018) 799–834.